Journal of The Electrochemical Society, 2020 **167** 050502

How Metallic Protection Layers Extend the Lifetime of NASICON-Based Solid-State Lithium Batteries

Francisco Javier Quintero Cortes,[1] John A. Lewis,[1] Jared Tippens,[2] Thomas S. Marchese,[1] and Matthew T. McDowell[1,2,*,z]

[1]*School of Materials Science and Engineering, Georgia Institute of Technology, Atlanta, Georgia 30332, USA*
[2]*George W. Woodruff School of Mechanical Engineering, Georgia Institute of Technology, Atlanta, Georgia 30332, USA*

The use of solid-state electrolytes (SSEs) within batteries is a promising strategy to safely access the high capacity of lithium metal anodes. However, most SSEs with practical ionic conductivity are chemically unstable in contact with lithium metal, which is detrimental to battery performance. Lithium aluminum germanium phosphate (LAGP) is an SSE with high ionic conductivity (10^{-4}-10^{-3} S cm^{-1}) and good environmental stability, but it forms an amorphous interphase region that continuously grows in contact with Li, leading to chemo-mechanical failure within solid-state batteries. Here, we find that thin (~30 nm) chromium interlayers deposited between the lithium electrode and LAGP extend cycle life to over 1000 h at moderate current densities (0.1–0.2 mA cm^{-2}), compared to ~30 h without protection. This significantly improved stability occurs because the metallic interlayer alters the trajectory of interphase formation and the nature of the electrochemical reaction at the interface. This work shows the promise of interface engineering for a variety of SSE materials within solid-state batteries, while emphasizing the necessity of understanding how protection layers affect dynamic evolution of interfaces.
 [DOI: 10.1149/2.0032005JES]

Manuscript submitted July 30, 2019; revised manuscript received September 24, 2019. Published October 11, 2019. *This paper is part of the JES Focus Issue on Heterogeneous Functional Materials for Energy Conversion and Storage.*

Solid state batteries (SSBs) are a promising alternative to conventional liquid-electrolyte-based cells for enabling high-capacity Li metal anodes, which have long carried safety risks when used in liquid electrolytes.[1,2] Replacing liquids with solid-state electrolytes (SSEs) reduces the risk of thermal runaway and may inhibit Li filamentary growth,[3] which could enable the use of Li metal anodes. Significant progress has been made in developing SSE materials with ionic conductivity >0.1 mS cm^{-1},[4–9] which is comparable to liquid electrolytes. However, most SSEs are thermodynamically unstable in contact with lithium metal, and they react to form new phases (an *interphase*) when in contact with Li.[10–12] In some cases, the growth of the interphase is kinetically limited and thus passivates the interface, which can result in relatively stable cycling.[13–15] In many SSEs with high ionic conductivity, such as some sodium super-ionic conductors (NASICON) and various sulfide Li-SSEs, the interphase is instead a mixed ionic-electronic conductor (MIEC).[16,17] MIEC interphases can grow continuously during cycling since both electrons and ions can be transported to react with the underlying SSE. The growth of such interphases can cause fracture of the SSE and cell failure, severely limiting operational current densities and cycle life for batteries with this type of SSE.[18–20]

NASICONs are attractive materials for SSBs despite the challenges they present. In contrast to sulfides and garnets, NASICONs such as $Li_{1+x}Al_xGe_{2-x}(PO_4)_3$ (LAGP) and $Li_{1+x}Al_xTi_{2-x}(PO_4)_3$ (LATP) are stable in ambient air and even in water.[21,22] As a consequence, processing is significantly simpler and more battery chemistries are enabled, such as Li-air batteries.[23] However, the interfacial reaction between some NASICON SSEs and Li generates a large volume expansion which causes mechanical degradation.[18,24] In the case of LAGP, it has been shown that the pristine material is continuously reduced, forming an amorphous interphase[18] containing metallic germanium.[16] The morphology of the interphase has been observed to play a key role in chemo-mechanical degradation and cell failure. At higher current densities (>~0.5 mA cm^{-2}), the interphase tends to grow with a filamentary morphology instead of the planar morphology found at lower current densities (~0.1 mA cm^{-2}), and fracture and failure are accelerated.[18] Using in situ X-ray tomography, we have shown that it is the mechanical degradation of LAGP that is responsible for cell failure due to increased impedance, rather than the impedance of the growing interphase itself.[19] With these recent findings in mind, it is clear that preventing or controlling the reaction process at the Li/SSE interface is critical for further development of these materials for Li metal SSBs.

The guiding principle to extend cycle life of unstable SSEs, including NASICON materials, is to prevent direct contact between Li and the SSE. This principle has led to the investigation of thin protection layers on SSEs,[25–31] layering of different SSEs,[32–34] and embedding the SSE into polymeric matrices.[35,36] These approaches have resulted in varying degrees of improvement in stability. In principle, the protective layer between Li metal and the SSE should enable ion transport but prevent electron transport to impede the electrochemical reduction of the SSE.[37,38] Surprisingly, electronically-conducting protective layer materials, such as Ge[29] and Al,[30] have recently been shown to significantly increase cycle life at moderate current densities (0.1–0.3 mA cm^{-2}) at room temperature. Despite this improved performance, there has been no comprehensive investigation of the underlying mechanisms by which these electronically-conducting protection layers improve stability.

Here, we demonstrate that thin Cr protection layers between Li and LAGP extend stable cycling times by more than an order of magnitude (from ~30 h to >1000 h), and we also show that this improved stability is due to altered morphological growth trajectories of the interphase instead of complete prevention of interphase growth. We attribute the observed uniform growth and improved chemo-mechanical stability of the interphase region to the ability of the vapor-deposited Cr films to mitigate non-uniformities in ion transport near the interface, which can cause irregular growth and cell failure. A variety of electrochemical techniques, in conjunction with X-ray photoelectron spectroscopy (XPS) and scanning electron microscopy (SEM), support these conclusions. Beyond demonstrating unprecedented electrochemical stability for the Li/LAGP interface, these results indicate that stable performance may be attained through interface engineering specifically designed to control interphase formation in a variety of unstable materials.

Experimental

Synthesis.—LAGP was synthesized following a procedure similar to that in our previously reported work.[18] 0.8 M germanium ethoxide (Alfa Aesar, 99.995%) and 0.2 M citric acid (Sigma-Aldrich, 99.5%) were mixed in deionized water at 80°C. After 20 h of stirring, stoichiometric amounts of lithium nitrate (Alfa Aesar, 99%), aluminum nitrate nonahydrate (Alfa Aesar, 98%) and ammonium phosphate (Sigma-Aldrich, 98%) were added to the solution. After 30 min, ethylene

*Electrochemical Society Member.
[z]E-mail: mattmcdowell@gatech.edu

glycol (Sigma-Aldrich, 99%) was added to the solution in a 1:1 molar ratio with citric acid (Sigma-Aldrich, 99%). Then, the temperature was sequentially raised to 120°C and 150°C and held for 30 min at each temperature. The mixture was then held at 170°C until dry. After drying, the powder was calcined and annealed in a tube furnace in ambient air at 500°C for 4 h and then 800°C for 5 h. The annealed powder was ball-milled and re-heated to 500°C for 4 h in order to burn off residue from the ball milling. The burnt-off powder was then ground using a mortar and pestle and uniaxially pressed into pellets. The pellets were sintered in air at 900°C for 6 h with a heating rate of 2°C min^{-1}. The pellets were polished using hexylene glycol (Allied) as a lubricant and diamond paper (Thorlabs) with grit sizes of 30 μm, 6 μm, 3 μm and 1 μm. After polishing, the pellets were heat treated at 675°C for 3 h with a heating rate of 2°C min^{-1}.

Protection layers.—Thin films of Cr were sputtered using a Unifilm Sputtering system. DC magnetron sputtering was performed under argon at a current of 0.045 A and a voltage of 98 V (approximate power of 4.41 W) using a 3-in Cr target (Kurt Lesker, 99.95%). The base pressure was below 8×10^{-6} Torr and the process pressure was 5×10^{-3} Torr. The deposition rate was fixed at 10 nm min^{-1} and the final thickness was typically 30 nm, although 5 nm and 60 nm were also used.

A custom-built ALD system was used to deposit thin films of Al_2O_3. Trimethyl aluminum (Sigma-Aldrich, 97%) and DI water were used as precursors, and nitrogen was used as the carrier gas. The process temperature was 150°C, the process pressure was 0.33 Torr, and the base pressure was below 0.06 Torr. The carrier gas flow rate was 20 sccm and the open and closed valve times for both precursors were 20 ms and 25 s, respectively. These conditions ensured a deposition rate of 1 Å per cycle. All depositions studied were run for 60 cycles.

Symmetric cells.—Bare and Cr-protected Li/LAGP/Li symmetric cells were fabricated using pellets that had been polished on both sides. In an argon-filled glove box, lithium disks (Sigma-Aldrich, 99.9%) with area of 0.486 cm^2 were cleaned and pressed on either side of the pellets. 2032 coin cells were assembled following this stack sequence: conducting foam, steel spacer, pellet with pressed lithium on both sides, steel spacer. The coin cells were pressed at 500 psi using a crimper. All symmetric cells were conditioned by cycling at 0.1 mA cm^{-2} for 5 min in each direction over 16 h. Electrochemical impedance spectra were collected in the range from 3 MHz to 2 Hz before and at different times during cycling using a Bio-Logic SP-200 potentiostat. Galvanostatic cycling (and conditioning) was completed using a Bio-Logic VMP3 potentiostat at room temperature.

Open-top cells.—Open-top cells were fabricated as shown in Figure 3a. Pellets polished on both sides and coated with 30 nm Cr or 30 nm Cr on 6 nm Al_2O_3 were used for open-top cells. Only one side of the pellet was initially in contact with a lithium disk of 0.486 cm^2 area, and the other side was open to the argon atmosphere in the glove box. A discharge current density of 0.1 mA cm^{-2} was applied for 50 min using a Bio-Logic VMP3 potentiostat at room temperature.

Full cells.—Bare and Cr-protected Li/LAGP/LFP full cells were fabricated using pellets that had been polished on one side. The solid-state $LiFePO_4$ (LFP, MTI Corp.) cathode was made from an acetonitrile (Sigma-Aldrich, 99.8%) slurry containing LFP, polyethylene oxide (PEO, 5 million M.W., Sigma-Aldrich), LiTFSI (Sigma-Aldrich, 99.95%), and Super P carbon powder (MTI). PEO and LiTFSI were dissolved in acetonitrile in an 8:1 molar ratio before mixing with the other components. The composition of the slurry was 20 wt% PEO-LiTFSI, 10 wt% Super P carbon powder, and 70 wt% LFP. The slurry was drop-cast onto the unpolished side of the LAGP pellet in the glove box, and a lithium disk was pressed onto the polished (bare or protected) side of the pellet. The full cells were galvanostatically cycled at a temperature of 60°C with voltage limits of 2.5 V and 4.0 V.

LAGP as electrode.—Half-cells with LAGP as the working electrode containing a liquid electrolyte were fabricated to study the electrochemistry of LAGP. LAGP slurries were made by mixing unsintered LAGP (70 wt%), Super P carbon powder (20 wt%), and PVDF-HFP (Kynar Flex) (10 wt%) in N-Methyl-2-Pyrrolidone (Sigma-Aldrich, 99.5%). The slurries were drop-cast on a copper foil and evenly spread using a doctor blade. Half-cells were made in 2032 coin cells using metallic lithium as the counter/reference electrode and 1.0 M $LiPF_6$ in 1:1 ethylene carbonate:diethyl carbonate (Sigma-Aldrich, battery grade) as the electrolyte. The cells were pressed and sealed inside an argon-filled glove box. Cyclic voltammetry (CV) and galvanostatic cycling were performed on these cells using a Bio-Logic VMP3 potentiostat at room temperature.

Characterization.—Symmetric and full cells were studied ex situ using scanning electron microscopy (SEM). Cross-sectional SEM images were obtained by breaking the LAGP pellet after cycling (whenever Cr was used) or by using the pieces from fractured pellets if fracture occurred during electrochemical cycling (this was common for bare LAGP). The samples were exposed to air for less than 20 s to transfer them into the SEM. Given the significant changes in morphology due to interphase growth (on the order of tens of microns), we do not expect the short air exposure to affect the interpretation of the SEM data. The instrument used was a Zeiss Ultra60 FE-SEM with an accelerating voltage of 5 or 10 kV.

The open-top cells were analyzed using X-ray photoelectron spectroscopy (XPS) to determine the presence of lithium on the surface of the pellets. XPS was performed using a Thermo Scientific K-Alpha system with a monochromatic Al Kα source. The spot size was 400 μm in diameter and the X-ray gun power was 15 W. The analyzer was set with a dwell time of 100 ms and a pass energy of 50 eV with a resolution of 0.05 eV. The surface of the sample was flooded with slow electrons and Ar^+ ions using the flood gun to compensate for surface charging. The base pressure was 4.5×10^{-8} Torr, and it never exceeded 1.8×10^{-7} Torr during analysis. All the samples were transferred from the glove box to the XPS chamber using a vacuum transfer holder that kept the sample sealed without exposure to air during the transfer.

Results and Discussion

As shown in Figure 1, the use of Cr as a protection layer significantly extends the cycling duration of symmetric Li/LAGP/Li cells. Without the Cr layer, the symmetric cell with bare LAGP cycled for a total of 25 h before reaching the voltage limit of 2 V (Figure 1a). In contrast, the symmetric cell with Cr on both sides of the LAGP cycled for 850 h at the same current density and similar overpotentials (Figure 1b). Our previous report on cycling of bare LAGP within symmetric cells also showed lifetimes of ∼30 h at current densities of 0.2 mA cm^{-2}.[18] Other protection layers, such as Al and Ge, have also shown improved cycling up to 200 h at current densities between 0.1 and 0.3 mA cm^{-2}.[29,30] We note that Cr is not expected to react with Li to form an alloy at room temperature,[39] as opposed to Al or Ge.[40–43] For this reason, we expect that Cr will remain as a thin film at the interface without reacting, and it will not diffuse into the Li metal electrode. The results in Figure 1b are among the longest cycling reported for LAGP in symmetric Li/Li cells at these moderate current densities, as seen in Table I. Figures 1c and 1d show magnified views of the galvanostatic curves from cycling at shorter times (Figure 1c) and longer times (Figure 1d). The shape of the curves with and without Cr are distinct in Figure 1c, with the Cr-free cell featuring flatter curves. The shape of the curves from the cell with Cr are relatively stable over time (Figure 1d).

Figure 1e shows electrochemical impedance spectra collected at different times during cycling of the Cr-protected cell in Figure 1b. The initial impedance spectra of bare and Cr-protected LAGP are very similar (Figure S1). Both exhibit one semicircle in the frequency space surveyed, which is typical for LAGP.[18,19] Total impedance is thus reported here since this metric defines the performance of the cells. The cell impedance remained relatively low during cycling and slowly

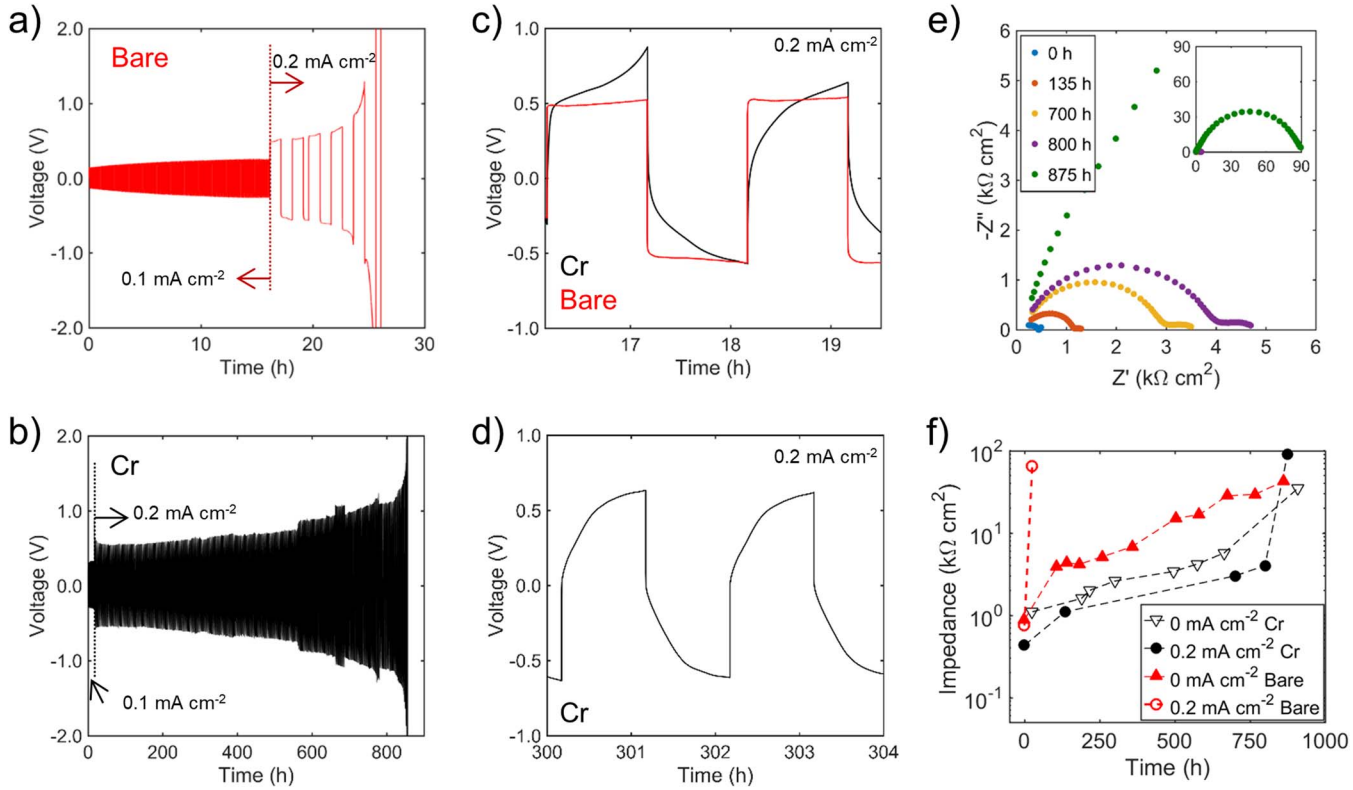

Figure 1. Electrochemistry of symmetric cells with and without Cr protection layers. a) Galvanostatic cycling of a symmetric Li/LAGP/Li cell with bare interfaces at 0.2 mA cm^{-2}. b) Galvanostatic cycling of a symmetric Li/LAGP/Li cell with 30 nm of Cr at both interfaces at 0.2 mA cm^{-2}. c, d) Magnified view of cycling of the two cells at different times, with (c) showing curves from both cells and (d) showing only the protected cell at longer times. e) Electrochemical impedance spectra of the cell presented in b collected at various times throughout cycling. f) Comparison of the evolution of total cell impedance over time among various cells, with the impedance plotted on a logarithmic scale. This plot shows the cell in panel (b) with 30 nm Cr interface layers cycled at 0.2 mA cm^{-2} (black circles), an identical cell through which no current was applied (empty triangles), a cell without any protection or current applied (red triangles), and an unprotected cell at 0.2 mA cm^{-2} (empty red circles).

increasing over time, but the impedance suddenly increased to ∼90 kΩ cm^2 over the last 75 h of cycling. This is likely due to mechanical fracture of the LAGP driven by the continuous formation of the interphase, as previously shown in unprotected cells.[18,19] Figure 1f shows the cell impedance over time for this Cr-protected cell and another Cr-protected cell with no current applied. This plot also shows impedance data from two different symmetric cells with bare interfaces; one was operated at 0.2 mA cm^{-2} and the other had no current applied. Interestingly, Figure 1f shows that the increase of impedance over time for the Cr-protected cell cycled at 0.2 mA cm^{-2} followed a trajectory similar to that of the identical cell without any current applied. In both cases, the impedance of these Cr-protected cells increases at

Table I. Performance benchmarks for protection layers in NASICON symmetric cells.

Solid Electrolyte	Protection Layer	Current Density (mA cm^{-2})	Temperature (°C)	Symmetric Cell Cycling Duration (h)	Reference
LAGP	Cr	0.2	RT	850	This work
LAGP	Cr on Al_2O_3	0.2	RT	1200	This work
LAGP	Ge	0.3	RT	200	29
LATP	BN + PEO* + PEGDE**	0.3	60	500	26
LATP	Modified Li SEI + Li_3PO_4 + liquid electrolyte	0.05	RT	200	27
LATP	Al_2O_3	0.01	RT	500	28
LATP	ZnO	0.2	RT	1000	44
LAGP	Amorphized LAGP	0.1	60	200	34
		1	80	40	
LAGP	LiPON	0.1	60	200	34
		1	80	40	
LAGP	Al	0.1	50	150	30

*PEO = Poly(ethylene oxide).
**PEGDE = Poly(ethylene glycol) dimethyl ether.
RT = Room temperature.

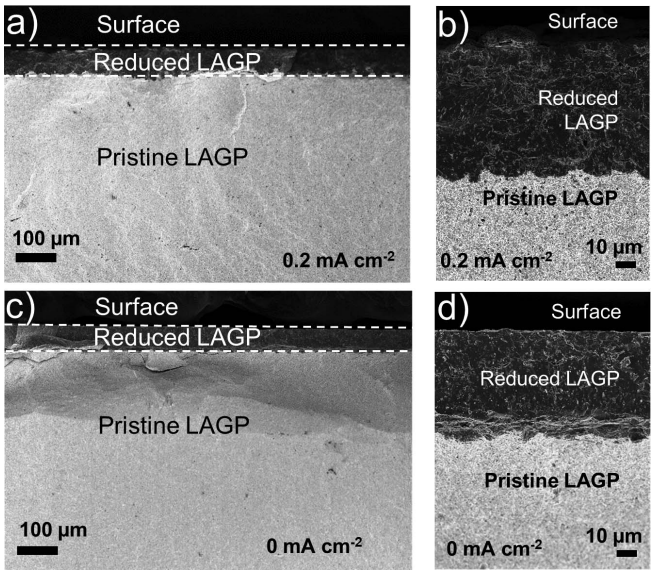

Figure 2. a, b) Cross-sectional SEM images of Cr-protected LAGP from a symmetric Li/LAGP/Li cell cycled at 0.2 mA cm^{-2} for 570 h at low magnification (a) and at high magnification (b). c, d) Cross-sectional SEM images of Cr-protected LAGP from an identical cell held for 660 h at open circuit.

roughly the same rate during the first ~650 h, resulting in a much higher impedance at the end of the experiments. The magnitude of the impedance of the Cr-protected cell at zero current is slightly higher than the cell at 0.2 mA cm^{-2} during the first ~650 h, but this is due to sample-to-sample variation. We note that interphase formation can still occur without applied current through direct chemical reaction, and bare LAGP has shown substantially improved chemo-mechanical stability under such conditions compared to when current is applied.[18] After ~850 h, the impedance of both cells without current and the Cr-protected cell under applied current were all of similar magnitude. These results are significant since they suggest that Cr-protected interfaces behave similarly both with and without an applied current, which differs from the unprotected case (bare cells with an applied current failed after 30 h, as shown in Figure 1f).

Additional investigation showed that the significantly increased stability is not due to the total prevention of reacted interphase formation by the Cr layers. Two identical symmetric cells with Cr-protected LAGP were constructed and tested under different conditions. One cell was cycled at 0.2 mA cm^{-2} for 570 h, and the other cell was held at open circuit without any applied current for 660 h. Figure 2 shows SEM images of the interphase region formed electrochemically (Figures 2a and 2b) and chemically (Figures 2c and 2d). The darker contrast of the interphase in the SEM images arises because of the higher electronic conductivity of the interphase and the incorporation of a significant amount of Li, which has a lower atomic number. The thickness and morphology of the interphase for both cells is very similar, which is consistent with the impedance evolution discussed in Figure 1f. In both cases, the interphase is uniform and planar, with a sharp reaction front separating it from the pristine LAGP. This information is important for two reasons. First, it is clear that the Cr layer does not prevent the chemical reaction even when no current is applied, which indicates that Li atoms can diffuse through the Cr interlayer and react with the underlying LAGP. Second, the uniform morphology of the interphase in Figure 2a is significantly different than the non-uniform interphase that forms under identical electrochemical conditions with unprotected LAGP.[18] Currents of 0.2 mA cm^{-2} in unprotected cells cause filamentary interphase morphologies, which results in mechanical stress concentrations that significantly accelerate chemo-mechanical degradation.[18] Uniform and planar interphases avoid these stress concentrations and can be stable for much longer times. We thus conclude that the Cr layer causes the interphase to grow much more uniformly than in unprotected cells under the same current conditions, and that this planar interphase morphology is responsible for the significantly improved electro-chemo-mechanical stability.

Despite this improved performance, Cr-protected symmetric cells cycled at higher currents were observed to exhibit shorter cycle life. *Post-mortem* cross-sectional SEM of Cr protected cells cycled at 0.3 mA cm^{-2} for over 120 h revealed filament-like interphase growth as well as interphase formation deep into the bulk of the pellet, which results in chemo-mechanical degradation and fracture (Figure S2). This indicates the existence of a current density limit above which the Cr layer no longer enables a uniform and planar reaction front to grow. The filament-like growth and the presence of interphase within the bulk of the pellet resembles the growth of Li filaments reported in garnets,[45,46] and the recent measurements of Li metal formation within the bulk of $Li_7La_3Zr_2O_{12}$ and Li_2S–P_2S_5.[47]

The interphase formation observed in the electrochemically-cycled sample in Figure 2 gives rise to an important question: is Li being plated/stripped, or is all the current being used for the electrochemical reaction of the SSE? It is difficult to determine the amount of Li plating/stripping solely from the electrochemical response in galvanostatic cycling of symmetric cells,[48] and the extended galvanostatic cycling thus does not directly translate into extended Li plating/stripping. To address this question, we designed an open-top cell, as depicted in the inset of Figure 3a. This cell was operated by applying current in one direction to cause reduction at the deposited Cr layer on the top side of the cell, which was exposed to the argon environment of a glove box. Both sides of the LAGP pellet were coated with the Cr layer, but only one side of the pellet was initially in contact with Li. With this cell, we can detect reaction products on the "open-top" side of the pellet without the presence of a thick Li foil electrode that obscures the solid-state interface. The Cr layer on the top of the pellet behaves as the electrical contact, and a thicker Cu ring is used as an electrical connection.

The electrochemical signatures from galvanostatic experiments with two different open-top cells are presented in Figure 3a. The black trace in Figure 3a is from an open-top cell with only a 30 nm Cr layer on top, while the blue trace is from an open-top cell with a bilayer of 30 nm Cr on top of 6 nm Al_2O_3 deposited by atomic layer deposition (ALD). For the cell with only Cr, the cell voltage remained above 0 V during the initial stages of the discharge and gradually fell below 0 V after 0.2 h. The XPS data shown in Figures 3b and 3c indicate that Li entirely covered the Cr layer, since the Cr 2p peaks are no longer visible after discharge. These data suggest that while there is some electrochemical reaction of the LAGP at higher potentials, there is also some Li metal deposition to cover the Cr layer. The cell with the Cr-Al_2O_3 bilayer was also constructed and tested to examine the effects of the electronically-insulating Al_2O_3 layer (which likely converts to a Li^+-conducting $LiAlO_x$ phase in contact with Li).[49–52] For this bilayer cell, the cell voltage immediately became negative under applied current in Figure 3a, and the voltage showed an initial dip typically associated with a nucleation overpotential.[53–55] This behavior suggests that this sample features direct electrochemical deposition of Li metal without significant reaction of the LAGP to form an interphase. However, the XPS data shown in Figures 3b and 3c show that Cr 2p peaks are detected after plating Li within this bilayer cell, which likely means that Li did not plate uniformly when the Al_2O_3 layer was added between Cr and LAGP. These results indicate that the initial electrochemical behavior of the interface can be directed through judicious choice of interfacial layers.

Although the Cr-Al_2O_3 bilayer enabled preferential lithium deposition without interphase formation in the early times of this experiment, long-term cycling still resulted in the reaction of LAGP and the formation of a uniform interphase. However, the dual layer also enabled a significant extension in cycle life in symmetric cells at a current density of 0.2 mA cm^{-2}, similar to Cr alone, as shown in Figure 3d. A 6 nm layer of Al_2O_3 alone at the interface did not result in improved stability (Figure 3d), indicating that the Cr layer was again necessary. Figure 3e shows that the interphase formed using the Cr-Al_2O_3

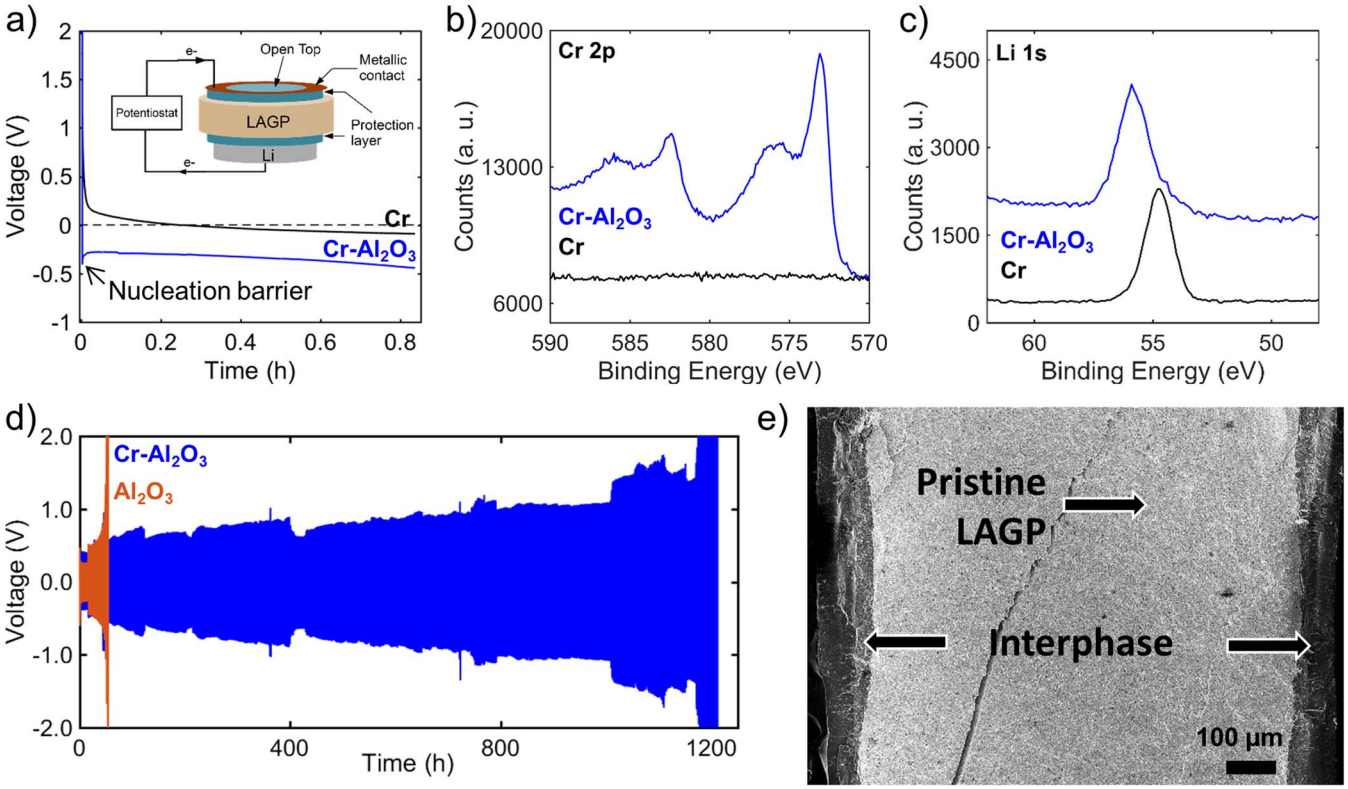

Figure 3. a) Schematic and data from the open-top cell experiments. The two curves show galvanostatic discharge of open-top cells at 0.1 mA cm^{-2} with 30 nm Cr (black) and 30 nm Cr on 6 nm Al_2O_3 (blue). b) Chromium 2p and c) lithium 1s XPS spectra of the open top surface after galvanostatic discharge of both samples. Deviations in peak positions of Li 1s are attributed to sample-to-sample variation, but the presence of Li species is verified with these results. d) Galvanostatic cycling from symmetric cells with the LAGP coated with either dual-layer Cr-Al_2O_3 (blue) or Al_2O_3 alone (orange). The Al_2O_3 was 6 nm in both cases, and the Cr was 30 nm. e) *Post-mortem* cross-sectional SEM of the Cr-Al_2O_3 protected cell after failure showing uniform interphase growth on both sides of the pellet.

dual layer during the experiment in Figure 3d is indistinguishable from that formed using Cr alone. We expect that the initial electron blocking effect that favors Li plating over LAGP reduction is lost over time as the Al_2O_3 transforms to a phase that is more electronically conducting, as well as because the Al_2O_3 layer can be mechanically damaged as the underlying LAGP reacts and expands to form the interphase. As the bilayer evolves to become more electronically conductive, LAGP reduction becomes more favored. In sum, a Cr-Al_2O_3 protection layer is not practically different from a Cr protection layer. We note that thicker Al_2O_3 layers were also tested within the bilayer, which significantly increased impedance (Figure S1).

Finally, we examined the effects of the Cr interfacial layer on the electrochemistry of full cells. The cathode in these cells consisted of $LiFePO_4$ (LFP) active material embedded in a poly(ethylene oxide) (PEO)-based polymer-electrolyte composite which was drop-cast on the top of the LAGP pellet (see Experimental). As shown in Figure 4, the Cr interfacial layer at the Li metal interface also extends stability of these full cells, and the full cells provide additional understanding of the behavior of these interfaces. Figure 4 shows the cycling behavior of Li/LAGP/LFP cells tested at 60°C using a current density of 0.1 mA cm^{-2}. The data from the Cr-protected LAGP cell in Figures 4b and 4c show much greater cycling stability than the data from the bare sample in Figure 4a. The extended cyclability attained with Cr is again connected to the improved chemo-mechanical stability of the LAGP pellet. Figure 4d shows that a planar, uniform interphase was formed on the anode side of a similar sample with no signs of fracture after 500 cycles. We believe that failure of these protected cells occurs not due to fracture, but due to delamination of the cathode (as can be seen in Figure 4d).

Another feature evident from Figures 4a and 4b is that the Cr interlayer alters the voltage of the full cell. As shown in Figures 4a and 4b, the galvanostatic curves of the Cr-protected LAGP cell consistently show lower charge/discharge voltages than the bare cells by about 0.3 V. The average voltage of ~3.4 V for the bare cell (Figure 4a) is consistent with the use of an LFP cathode and Li plating/stripping at the anode. The reduction in cell voltage for the Cr-coated cell is most likely due to the negative electrode reaction being reversible conversion of the LAGP instead of Li plating/stripping. To further investigate this possibility, we constructed conventional slurry-based electrodes with LAGP powder and examined their electrochemical behavior within liquid-electrolyte half cells (see Experimental section). Cyclic voltammetry and galvanostatic cycling of LAGP working electrodes showed that this material undergoes redox (likely a conversion reaction) between about 0.2 and 0.4 V vs. Li/Li^+ (Figure S3). These additional results provide strong evidence that the shift in voltage of the Cr-protected solid-state cell in Figure 4b is due to reversible conversion reaction of the LAGP at the anode. Thus, these findings suggest that without the Cr protection layer, Li/LAGP/LFP full cells operate via Li plating/stripping at the anode, but when the Cr layer is added, it promotes the direct electrochemical conversion reaction of the LAGP. In the Cr-protected LAGP cells, the Cr layer represents an additional barrier for Li transport, which could frustrate Li plating/stripping and favor electrochemical conversion. These findings are largely consistent with the open-top cell shown in Figure 3a, in which reduction occurred above 0.0 V vs. Li/Li^+. However, the XPS observation of coverage of the Cr layer in Figure 3c suggested at least some Li deposition, which could have occurred because of the open space above Cr in this configuration or the different electrochemical nature of the cell.

As shown herein, the addition of the sputtered Cr film caused the interphase to grow in a very uniform and planar fashion at current densities up to 0.2 mA cm^{-2}, which is in contrast to filamentary growth

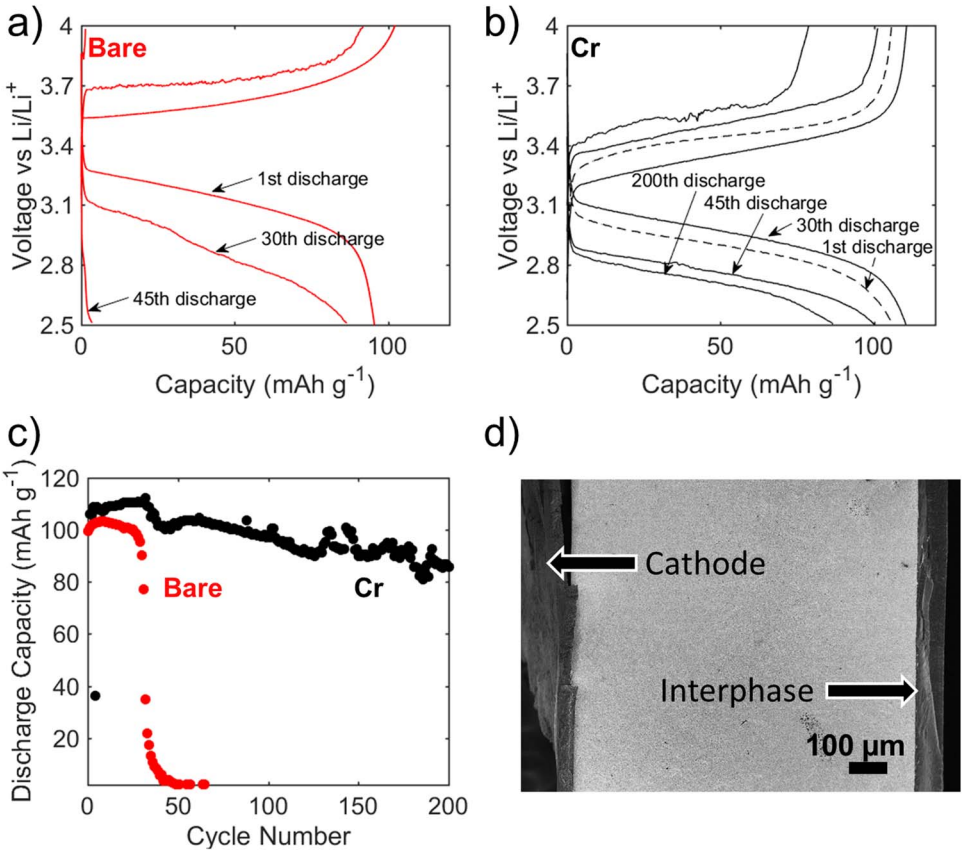

Figure 4. Characterization of full cells with a $LiFePO_4$ cathode. a) Galvanostatic charge/discharge curves at 0.1 mA cm^{-2} from a Li/LAGP/LFP cell with uncoated interfaces. b) Galvanostatic charge/discharge curves at 0.1 mA cm^{-2} from a Li/LAGP/LFP cell with the Li interface coated with 30 nm of Cr. The cells in (a) and (b) were tested at 60°C. c) Discharge capacity for the cells in (a) and (b). d) *Post-mortem* cross-sectional SEM image of a protected cell after cycling for 500 cycles.

in bare cells which leads to chemo-mechanical degradation and cell failure. We propose that the significantly improved stability of the cells with Cr-coated interfaces, as well as the differences in electrochemical behavior in full cells, are due to the Cr layer acting to remove electric field concentrations and other sources of ionic current "hot-spots" at the interface. The improved physical contact and coverage of the vapor-deposited Cr film compared to a pure Li electrode on the LAGP surface is one probable source of this behavior, as it removes point contacts present when using Li foils that could result in electric field/ionic current concentrations and filamentary interphase growth.[56] Sputter deposition of the Cr creates a uniform film in intimate contact with the polished polycrystalline LAGP surface. The Li electrodes, on the other hand, are bulk foils that are much rougher and exhibit non-uniform contact at the LAGP surface. This argument also explains the success of other reported vapor-deposited protection layers, such as Ge.[29] Finally, it is also possible that these various metal interlayers impact charge transfer and interphase growth trajectories via altering the partial molar volume of Li, as has been predicted previously.[57]

At higher current densities, filamentary growth of the interphase occurs following a mechanism similar to that reported for bare LAGP.[18] Beyond 0.2 mA cm^{-2}, the rate of reaction is accelerated and minor irregularities due to surface roughness or grain boundaries create preferential pathways for ionic transport and interphase formation. We hypothesize that, while electron transport can be uniform due to the metallic Cr protection layer, Li^+ transport is still restricted due to imperfect contact, which can lead to preferential localized growth of the interphase. Since the interphase is a MIEC,[16,17] reduction of pristine LAGP is favored at the interphase protrusions, where the ion transport distance is shorter.[18] It is possible that higher pressures[58] or other strategies to improve contact at the interface could improve stability at higher current densities.

Conclusions

This work shows that metallic protection layers can enable >1000 h of cycling time for NASICON-based lithium metal batteries, and it provides important insights into the mechanisms through which these metallic protection layers operate. We demonstrate that engineering the Li-SSE interface with metallic layers enables control over the evolution of the interphase, which is key for the long-term stability of LAGP. Cr interlayer films were found to significantly extend the lifetime of symmetric and full cells by promoting uniform interphase growth and delaying fracture at moderate current densities. At the same time, the Cr layers promoted reversible electrochemical conversion of the LAGP material instead of Li deposition/stripping. Experiments with electron-blocking Cr-Al_2O_3 bilayers showed initial promotion of Li plating, but long-term stability and interphase growth were similar Cr alone. These results are important since they demonstrate the underlying mechanisms that govern the action of metallic protection layers. In particular, the ability of the 30 nm Cr layers to allow Li^+ to be transported while also reducing ion transport non-uniformities and improving stability could be beneficial when used with a variety of SSE materials. For ultimate stability, however, true electron-blocking layers to entirely prevent interphase formation, or other layers that can significantly slow the growth of the interphase, are seemingly required. In either case, the use of metallic layers in conjunction with these future protection materials could be advantageous. Thus, we expect that the findings reported here are an important step on the way toward the development of a diverse array of solid-state battery chemistries with long-term stability and high energy.

Acknowledgments

This material is based upon work supported by the National Science Foundation under Award No. DMR-1652471. This work was performed in part at the Georgia Tech Institute for Electronics and Nanotechnology, a member of the National Nanotechnology Coordinated Infrastructure, which is supported by the National Science Foundation (grant ECCS-1542174). F.J.Q.C. acknowledges support from Colciencias-Fulbright scholarship program cohort 2016.

ORCID

Francisco Javier Quintero Cortes https://orcid.org/0000-0002-7019-3675
Matthew T. McDowell https://orcid.org/0000-0001-5552-3456

References

1. U. von Sacken, E. Nodwell, A. Sundher, and J. R. Dahn, *J. Power Sources*, **54**, 240 (1995).
2. R. Bhattacharyya, B. Key, H. Chen, A. S. Best, A. F. Hollenkamp, and C. P. Grey, *Nat. Mater.*, **9**, 504 (2010).
3. Y. Kato, S. Hori, T. Saito, K. Suzuki, M. Hirayama, A. Mitsui, M. Yonemura, H. Iba, and R. Kanno, *Nat. Energy*, 1 (2016).
4. N. Kamaya, K. Homma, Y. Yamakawa, M. Hirayama, R. Kanno, M. Yonemura, T. Kamiyama, Y. Kato, S. Hama, K. Kawamoto, and A. Mitsui, *Nat. Mater.*, **10**, 682 (2011).
5. H. Aono, E. Sugimoto, Y. Sadaoka, N. Imanaka, and G. Adachi, *J. Electrochem. Soc.*, **137**, 1023 (1990).
6. J. Wolfenstine, J. Ratchford, E. Rangasamy, J. Sakamoto, and J. L. Allen, *Mater. Chem. Phys.*, **134**, 571 (2012).
7. R. Murugan, V. Thangadurai, and W. Weppner, *Angew. Chem. Int. Ed.*, **46**, 7778 (2007).
8. K. Kerman, A. Luntz, V. Viswanathan, Y. Chiang, and Z. Chen, *J. Electrochem. Soc.*, **167**, A1731 (2017).
9. M. Kotobuki, H. Munakata, K. Kanamura, Y. Sato, and T. Yoshida, *J. Electrochem. Soc.*, **157**, A1076 (2010).
10. N. Riphaus, B. Stiaszny, H. Beyer, S. Indris, H. A. Gasteiger, and S. S. J. Sedlmaier, *J. Electrochem. Soc.*, **166**, A975 (2019).
11. Y. Zhu, X. He, and Y. Mo, *ACS Appl. Mater. Interfaces*, **7**, 23685 (2015).
12. V. Augustyn, M. T. McDowell, and A. Vojvodic, *Joule*, **2**, 2189 (2018).
13. C. Ma, Y. Cheng, K. Yin, J. Luo, A. Sharafi, J. Sakamoto, J. Li, K. L. More, N. J. Dudney, and M. Chi, *Nano Lett.*, **16**, 7030 (2016).
14. A. Sharafi, H. M. Meyer, J. Nanda, J. Wolfenstine, and J. Sakamoto, *J. Power Sources*, **302**, 135 (2016).
15. S. Wenzel, D. A. Weber, T. Leichtweiss, M. R. Busche, J. Sann, and J. Janek, *Solid State Ionics*, **286**, 24 (2016).
16. P. Hartmann, T. Leichtweiss, M. R. Busche, M. Schneider, M. Reich, J. Sann, P. Adelhelm, and J. Janek, *J. Phys. Chem. C*, **117**, 21064 (2013).
17. S. Wenzel, S. Randau, T. Leichtweiß, D. A. Weber, J. Sann, W. G. Zeier, and J. Janek, *Chem. Mater.*, **28**, 2400 (2016).
18. J. A. Lewis, F. J. Q. Cortes, M. G. Boebinger, J. Tippens, T. S. Marchese, N. Kondekar, X. Liu, M. Chi, and M. T. McDowell, *ACS Energy Lett.*, **4**, 591 (2019).
19. J. Tippens, J. C. Miers, A. Afshar, J. A. Lewis, F. J. Q. Cortes, H. Qiao, T. S. Marchese, C. V. Di Leo, C. Saldana, and M. T. McDowell, *ACS Energy Lett.*, **4**, 1475 (2019).
20. J. A. Lewis, J. Tippens, F. J. Q. Cortes, and M. T. McDowell, *Trends Chem.* (2019).
21. K. He, C. Zu, Y. Wang, B. Han, X. Yin, H. Zhao, Y. Liu, and J. Chen, *Solid State Ion.*, **254**, 78 (2014).
22. M. Zhang, K. Takahashi, N. Imanishi, Y. Takeda, O. Yamamoto, B. Chi, J. Pu, and J. Li, *J. Electrochem. Soc.*, **159**, A1114 (2012).
23. H. Kitaura and H. Zhou, *Energy Environ. Sci.*, **5**, 9077 (2012).
24. H. Chung and B. Kang, *Chem. Mater.*, **29**, 8611 (2017).
25. M. Nagao, A. Hayashi, and M. Tatsumisago, *Electrochemistry*, **80**, 734 (2012).
26. Q. Cheng, A. Li, N. Li, S. Li, A. Zangiabadi, T.-D. Li, W. Huang, A. C. Li, T. Jin, Q. Song, W. Xu, N. Ni, H. Zhai, M. Dontigny, K. Zaghib, X. Chuan, D. Su, K. Yan, and Y. Yang, *Joule*, **3**(6), 1510 (2019).
27. J. Liu, T. Liu, Y. Pu, M. Guan, Z. Tang, F. Ding, Z. Xu, and Y. Li, *RSC Adv.*, **7**, 46545 (2017).
28. Y. Liu, Q. Sun, Y. Zhao, B. Wang, P. Kaghazchi, K. R. Adair, R. Li, C. Zhang, J. Liu, L.-Y. Kuo, Y. Hu, T.-K. Sham, L. Zhang, R. Yang, S. Lu, X. Song, and X. Sun, *ACS Appl. Mater. Interfaces*, **10**, 31240 (2018).
29. Y. Liu, C. Li, B. Li, H. Song, Z. Cheng, M. Chen, P. He, and H. Zhou, *Adv. Energy Mater.*, **8**, 1702374 (2018).
30. H. Zhong, L. Sang, F. Ding, J. Song, and Y. Mai, *Electrochim. Acta*, **277**, 268 (2018).
31. X. Han, Y. Gong, K. Fu, X. He, G. T. Hitz, J. Dai, A. Pearse, B. Liu, H. Wang, G. Rubloff, Y. Mo, V. Thangadurai, E. D. Wachsman, and L. Hu, *Nat. Mater.*, **16**, 572 (2017).
32. E. Zhao, F. Ma, Y. Guo, and Y. Jin, *RSC Adv.*, **6**, 92579 (2016).
33. H. S. Jadhav, R. S. Kalubarme, A. H. Jadhav, and J. G. Seo, *Electrochim. Acta*, **199**, 126 (2016).
34. Z. Zhang, S. Chen, J. Yang, G. Liu, X. Yao, P. Cui, and X. Xu, *Electrochim. Acta*, **297**, 281 (2019).
35. C. Wang, Y. Yang, X. Liu, H. Zhong, H. Xu, Z. Xu, H. Shao, and F. Ding, *ACS Appl. Mater. Interfaces*, **9**, 13694 (2017).
36. D. Bosubabu, J. Sivaraj, R. Sampathkumar, and K. Ramesha, *ACS Appl. Energy Mater.*, **2**(6) 4118 (2019).
37. Y. Zhu, X. He, and Y. Mo, *Adv. Sci.*, **4**, 1600517 (2017).
38. A. M. Nolan, Y. Zhu, X. He, Q. Bai, and Y. Mo, *Joule*, **2**, 2016 (2018).
39. M. Venkatraman and J. P. Neumann, *Bull. Alloy Phase Diagrams*, **5**, 399 (1984).
40. L. F. Mondolfo, *Aluminum Alloys*, 308 (1976).
41. J. Sangster and A. D. Pelton, *J. Phase Equilibria*, **18**, 289 (1997).
42. M. H. Tahmasebi, D. Kramer, R. Mönig, and S. T. Boles, *J. Electrochem. Soc.*, **166**, A5001 (2019).
43. F. J. Q. Cortes, M. G. Boebinger, M. Xu, A. Ulvestad, and M. T. McDowell, *ACS Energy Lett.*, **3**, 349 (2018).
44. X. Hao, Q. Zhao, S. Su, S. Zhang, J. Ma, L. Shen, Q. Yu, L. Zhao, Y. Liu, F. Kang, and Y. He, *Adv. Energy Mater.*, **9**, 1901604 (2019).
45. Y. Ren, Y. Shen, Y. Lin, and C.-W. Nan, *Electrochem. Commun.*, **57**, 27 (2015).
46. L. Porz, T. Swamy, B. W. Sheldon, D. Rettenwander, T. Frömling, H. L. Thaman, S. Berendts, R. Uecker, W. Craig Carter, and Y.-M. Chiang, *Adv. Energy Mater.*, **7**, 1701003 (2017).
47. F. Han, A. S. Westover, J. Yue, X. Fan, F. Wang, M. Chi, D. N. Leonard, N. J. Dudney, H. Wang, and C. Wang, *Nat. Energy*, **4**, 187 (2019).
48. K.-H. Chen, K. N. Wood, E. Kazyak, W. S. LePage, A. L. Davis, A. J. Sanchez, and N. P. Dasgupta, *J. Mater. Chem. A*, **5**, 11671 (2017).
49. S. C. Jung and Y.-K. Han, *J. Phys. Chem. Lett.*, **4**, 2681 (2013).
50. S.-T. Myung, K. Izumi, S. Komaba, Y.-K. Sun, H. Yashiro, and N. Kumagai, *Chem. Mater.*, **17**, 3695 (2005).
51. V. Miikkulainen, O. Nilsen, H. Li, S. W. King, M. Laitinen, T. Sajavaara, and H. Fjellvåg, *J. Vac. Sci. Technol. A.*, **33**, 01A101 (2015).
52. E. Kazyak, K. N. Wood, and N. P. Dasgupta, *Chem. Mater.*, **27**, 6457 (2015).
53. K. Yan, Z. Lu, H.-W. Lee, F. Xiong, P.-C. Hsu, Y. Li, J. Zhao, S. Chu, and Y. Cui, *Nat. Energy*, **1**, 16010 (2016).
54. K. N. Wood, E. Kazyak, A. F. Chadwick, K.-H. Chen, J.-G. Zhang, K. Thornton, and N. P. Dasgupta, *ACS Cent. Sci.*, **2**, 790 (2016).
55. T. Krauskopf, R. Dippel, H. Hartmann, K. Peppler, B. Mogwitz, F. Richter, W. G. Zeier, and J. Janek, *Joule*, **3**, 1 (2019).
56. T. Krauskopf, H. Hartmann, W. G. Zeier, and J. Janek, *ACS Appl. Mater. Interfaces*, **11**, 14463 (2019).
57. Z. Ahmad and V. Viswanathan, *Phys. Rev. Lett.*, **119**, 056003 (2017).
58. M. J. Wang, R. Choudhury, and J. Sakamoto, *Joule*, (2019).